UCRL-JC-124529
PREPRINT

Third-Harmonic Performance of the Beamlet Prototype Laser

P. J. Wegner, C. E. Barker, J. A. Caird,
S. N. Dixit, M. A. Henesian, L. G. Seppala,
C. E. Thompson, and B. V. Van Wonterghem

This paper was prepared for submittal to the
2nd Annual International Conference on Solid-State
Lasers for Application to Inertial Confinement Fusion
Paris, France
October 22-25, 1996

January 31, 1997

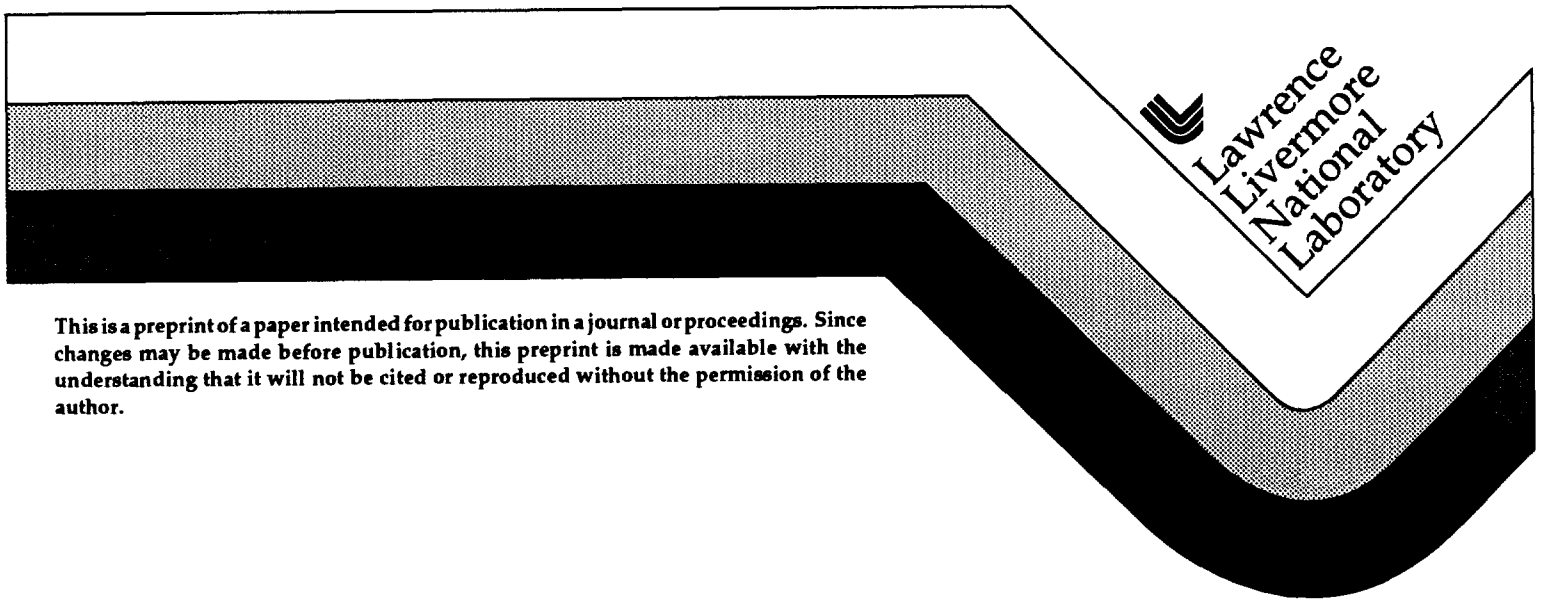

This is a preprint of a paper intended for publication in a journal or proceedings. Since changes may be made before publication, this preprint is made available with the understanding that it will not be cited or reproduced without the permission of the author.

DISCLAIMER

This document was prepared as an account of work sponsored by an agency of the United States Government. Neither the United States Government nor the University of California nor any of their employees, makes any warranty, express or implied, or assumes any legal liability or responsibility for the accuracy, completeness, or usefulness of any information, apparatus, product, or process disclosed, or represents that its use would not infringe privately owned rights. Reference herein to any specific commercial product, process, or service by trade name, trademark, manufacturer, or otherwise, does not necessarily constitute or imply its endorsement, recommendation, or favoring by the United States Government or the University of California. The views and opinions of authors expressed herein do not necessarily state or reflect those of the United States Government or the University of California, and shall not be used for advertising or product endorsement purposes.

Third-harmonic performance of the Beamlet prototype laser

P. J. Wegner, C. E. Barker, J. A. Caird, S. N. Dixit, M. A. Henesian,
L. G. Seppala, C. E. Thompson and B. M. Van Wonterghem

Lawrence Livermore National Laboratory
PO Box 5508, Livermore, CA, 94550

ABSTRACT

The Beamlet laser is a nearly full-scale, single-aperture prototype of the driver design for the National Ignition Facility (NIF). As part of a test and validation plan for the NIF design, Beamlet was recently equipped with final focussing optics and diagnostics for the purpose of evaluating integrated component performance and equivalent target-plane irradiance conditions at the 0.351-μm output wavelength specified for NIF targets. A 37-cm aperture two-crystal converter scheme generates the third harmonic of the Nd:glass 1.053-μm wavelength with high efficiency. The efficiency of the converter has been characterized and is reported, along with detailed measurements of the near-field and far-field UV irradiance distributions at operating conditions up to and exceeding red-line levels for the NIF. Dependences of observed beam quality on critical laser parameters including output power, B-integral, and spatial filtering are discussed and compared with numerical simulations.

1. INTRODUCTION

The inertial confinement fusion (ICF) mission for the National Ignition Facility requires that each of the 192 beams of the driver deliver 9 kJ of 0.351-um energy on target with a peak power of 2.6 TW [1]. Increased power levels of up to 4 TW have additionally been specified for tests related to science-based stockpile stewardship (SBSS) [2]. Both missions specify that the laser power be delivered to the target in a controlled fashion, thus setting limits on the amount of beam divergence that can be produced by the driver. Divergence specifications for ICF require that 95% of the power be delivered inside a half-angle of 43 μrad. The specification includes allowances for the diffraction efficiency of a kinoform phase plate which is used to shape the profile of the focal spot[3]. The divergence goal that has been adopted for the SBSS mission is much more stringent, calling for 80% of the power (3.2 TW) to be delivered inside a half angle of 14 μrad. For the purpose of this discussion, sources of driver divergence are separated into two sections: the 1.053-μm (1ω) laser and the 0.351-μm (3ω) optics, including the frequency converter. Divergence associated with the 1ω laser has been well-characterized through detailed studies performed on the Beamlet prototype laser [4-7]. Low-frequency wavefront errors are known to originate in the 1ω laser that are both static and pump-induced; these errors are partially corrected using adaptive optics [4,7,8]. Higher-frequency wavefront errors originating from optical scattering- both linear and nonlinear- are partially controlled through spatial filtering [5,6]. Divergence issues associated with the 3ω optics are not as well-characterized. The efficiency of the frequency converter, for example, is known to depend on the 1ω divergence. The divergence of the 1ω beam is transferred to the 3ω beam in a complex manner in the frequency converter, with ripple transfer theory predicting a factor of 9 gain in power for certain types of phase noise [9]. In addition, the diamond-turned surfaces of the converter crystals act as a source of high-frequency noise that is a potential seed for nonlinear scattering in the final optics, where the threshold for 3ω filamentation is expected to be a factor of three to four lower than the corresponding threshold at 1ω [10,11].

We have recently conducted a series of tests on the Beamlet to measure its 3ω performance under operating conditions that are relevant to the NIF. The purpose of the tests was to evaluate the efficiency of the frequency converter and the quality of the output beam at power levels and B-integrals up to and exceeding NIF design levels. The goals of the tests were threefold: first, to determine whether current crystal specifications and the quality of the 1ω beam produced on the Beamlet are adequate for converting peak power to the third harmonic with >80% efficiency. Whole-beam energy efficiencies of 80% were previously demonstrated on the Beamlet, however those results were obtained using a reduced beam size of 30 cm with 32-cm aperture crystals [4]. Second, we wished to quantify Beamlet's operating margin against 3ω filamentation and ascertain whether current specifications for the roughness of the crystal surfaces are adequate to mitigate this effect. And third, we wanted to determine

amplifiers cavity-booster	spatial filters cavity/transport (μrad)	$\Sigma B_{1\omega}$ (radians)	$P_{3\omega}$ (TW)
11-0	130/100	0.9 - 3.6	0.4 - 2.6
11-0	200/200	0.8 - 2.8	0.4 - 2.2
11-5	130/200	1.6 - 2.2	2.8 - 3.7

Table 1. Parameter space investigated in the Beamlet 3ω tests

whether Beamlet can meet NIF focal-spot specifications, and identify any required improvements in beam quality. Test parameters were designed to simulate NIF conditions as closely as possible. The frequency converter used in the tests was of a two-crystal design identical to that adopted for the NIF, consisting of type-I doubling in 10.5 mm of KDP followed by type-II sum-frequency mixing in 9.5 mm of deuterated KDP (KD*P) [12-14]. The crystals were 37-cm prototypes of the 40-cm NIF crystals, finished to a surface roughness of < 20 Angstroms RMS prior to the tests to be consistent with NIF specifications for optical quality. A square f/20 silica lens was used to focus the 3ω beam at an equivalent target plane located inside a vacuum vessel that also housed the 1-meter aperture sampling optics for the diagnostics [10]. The lens had an off-axis design for angularly dispersing the1ω, 2ω and 3ω radiation, that caused its thickness to vary from 1 to 4.8 cm across the aperture. The beam size used in the tests was 34 cm (1% intensity level) with an equivalent area of 1010 cm^2, which is currently the largest beam that can be propagated through Beamlet's cavity switch.

The pulse format for the tests was 200-ps Gaussian, which proved advantageous for several reasons. First, the relatively short pulse duration made it possible to reach the high peak powers and irradiance levels important for investigating frequency conversion, nonlinear propagation effects, and beam quality, while restricting fluence to modest levels. This was important because as in past ICF laser designs, the 3ω lens on the Beamlet forms a pressure barrier for a vacuum chamber. With 3ω fluences on the NIF expected to approach 9 J/cm^2 average, the resulting safety factor of ~2 relative to the measured damage threshold of the lens was deemed inadequate for a pressure barrier, and the NIF design now calls for a vacuum window to be located in the 1ω beam path upstream of the frequency converter, where the damage threshold of the component will be significantly higher. High-fluence testing of the Beamlet lens could thus not be justified at this time, and has been postponed until a more NIF-like final optics configuration can be implemented on the facility. Second, the use of short pulses was preferred for these tests because we wished to measure near-field and far-field beam quality with imaging diagnostics that integrate over the duration of the pulse (scientific grade CCD arrays, for example). With the longer pulses typical of ICF applications, gain saturation in the laser amplifier cause B-integral to increase and beam quality to decrease in time through the pulse, an effect that would be masked by a time-integrated measurement. We therefore used short pulses and adjusted the gain of the laser amplifier to simulate propagation conditions in a long pulse and obtain a "snap shot" of beam quality for the time slice of interest. To simulate the highly-saturated, high B-integral conditions that exist at the end of a shaped 20-ns ICF ignition pulse, we conducted the majority of these tests with the booster amplifiers turned off. As summarized in Table I, this method allowed us to achieve a total B-integral in the main cavity and booster amplifier stages of up to 3.6 radians (ΣB) , at output 3ω power levels of up to 2.6 TW. To test the higher-power, shorter-pulse conditions required for SBSS applications we activated the booster amplifiers and attained output powers of up to 3.7 TW at substantially lower B-integral.

Specific results from these tests are summarized in the following three sections. The efficiency of the frequency converter and issues related to the first goal of these tests are covered in Section 2. Sections 3 and 4 cover measurements of near-field and far-field beam quality, and address the second and third test objectives concerning 3ω filamentation and focal-spot characterization, respectively.

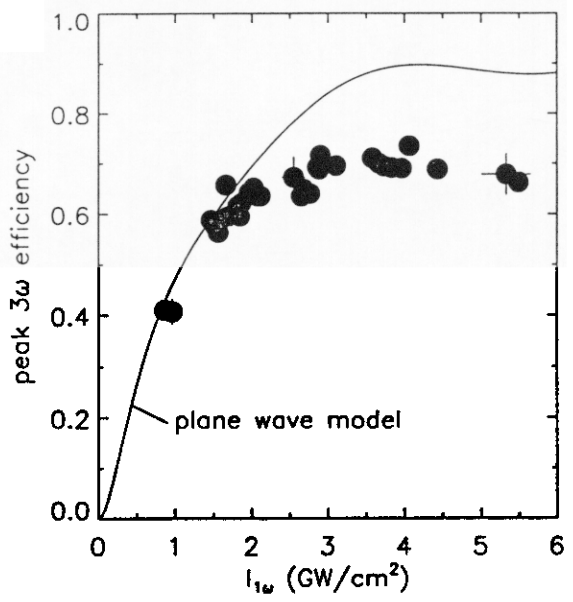

Figure 1(a). Measured peak-power third-harmonic efficiency of the 37-cm frequency converter, plotted versus peak 1ω drive irradiance. Plane-wave theory shown for comparison.

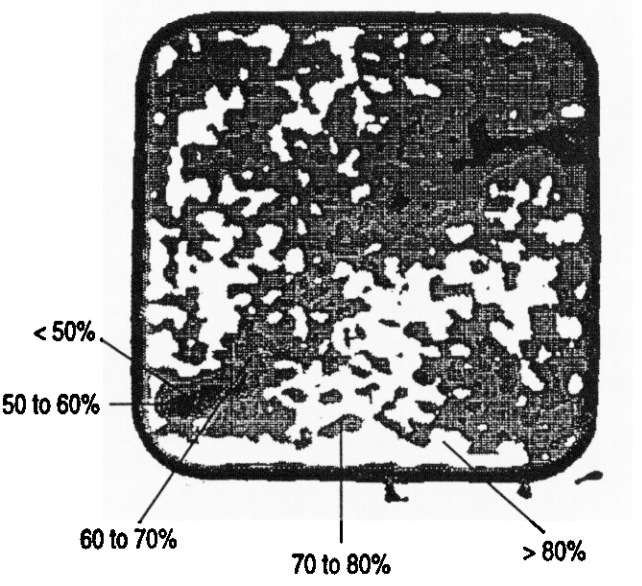

Figure 1(b). Spatial variation in conversion efficiency measured across the 34-cm beam, at a peak 1ω drive power of 4.3 TW. 25% of the beam area is converted with greater than 80% efficiency.

2. CONVERSION EFFICIENCY

The efficiency of the frequency converter was evaluated by measuring the 3ω energy and pulse shape exiting the final focus lens and comparing it to the corresponding 1ω pulse parameters incident on a silica beam splitter located immediately upstream of the crystals. The second surface of the beam splitter and both surfaces of the focus lens were anti-reflection coated and contributed only a small uncertainty to the measurement. The 1ω energy was measured with a calorimeter having an absolute accuracy of ± 3% and an angular field of view exceeding that of the transport spatial filter pinhole. The 3ω calorimetry had similar accuracy and a field of view exceeding ± 2 mrad. Residual 1ω and 2ω energy levels were monitored with diodes to ascertain energy balance within a few percent; both the diodes and the 3ω calorimeter were calibrated by reference to a full-aperture calorimeter situated in the vacuum chamber on shots designed to pass only one wavelength. Pulse shapes at 1ω and 3ω were measured on the same streak camera to reduce uncertainty in the efficiency calculations. The effective 1ω pulse width, defined to be the pulse duration which when divided into the energy yields peak power, was measured to be 235 ± 5 ps. The effective 3ω pulse width varied from 195 to 230 ps, depending on drive power and crystal tuning.

Measurements revealed that the overall efficiency of the Beamlet 37-cm frequency converter is limited by spatial non-uniformity. As shown in Figure 1(a), the total peak power contained inside the beam aperture was converted with less than 74% efficiency. The efficiencies plotted in the figure represent the measurement of spatially-averaged quantities, i.e. total pulse energy and aperture-averaged pulse shape. When a spatially-resolved analysis was performed using measured near-field irradiance distributions it was discovered that the conversion efficiency varied significantly across the aperture. Figure 1(b) shows a spatial map of the peak-power efficiency measured on a 4.3 TW peak-power shot that generated 3.1 TW at the third harmonic. The measurement shows that while ~25% of the beam area converted with >80% efficiency, a substantial fraction of the beam area converted with less than 70% efficiency, yielding an average efficiency for the aperture of only 72%. Improved spatial uniformity could be obtained by adjusting the tuning of the doubling crystal, but at the cost of lower overall efficiency.

The observed spatial variations in efficiency point to non-uniformity of the crystal quality or birefringence. Using plane-

wave theory we have estimated the angular detuning that would be required to produce the measured 3ω near-field irradiance distributions from the measured 1ω irradiance distributions. For the detuning to occur entirely in the tripler, a variation in phase match angle across the crystal of ~350 μrad would be required; a fairly large detuning, but one that could be realized by a few-percent variation in the crystal deuteration level [15]. On the other hand, only a 50-μrad shift in phase matching angle is needed to produce the same effect in the doubler. Furthermore, transmission interferograms of the doubler obtained with unpolarized light exhibit several features in the refractive index with a pattern similar to that shown in Figure 1(b) [14]. As part of the NIF frequency converter development effort, a comprehensive set of tests is now underway to evaluate crystal homogeneity and its impact on harmonic generation. The measurements include linearly-polarized interferometry to map crystal refractive index for orthogonal polarizations, spatially-resolved polarimetry to map the orientation of the crystal axes, and stoichiometry of plates cut from the original boules of material to evaluate deuteration level. Code development is also underway to incorporate spatially varying birefringence in the model for the frequency converter.

3. NEAR FIELD BEAM QUALITY

The measurements of 3ω beam quality were designed to address two angular regimes that are manifested in the near field by beam structure of very different scale lengths. To illustrate, a small patch of the 3ω beam sampled at a plane one meter downstream of the converter is expected to have an irradiance distribution similar to that of the simulation shown in Figure 2, which depicts a nominally centimeter scale-length bump or ripple superposed with ripple of much finer scale. The fine-scale structure of concern corresponds to angular content of order ~ 0.5 mrad or greater, and has its primary source in the diamond-turned surfaces of the converter crystals. Fractional energy in this angular regime has the disadvantage that it reduces the transport efficiency of the driver (misses the target) and acts as a seed for nonlinear scattering in the final optics [10]. The larger scale-length structure evident in the simulation represent angles of 200 μrad or less that lie within the passband of the 1ω spatial filters. Modulation at this scale length and its dependence on output power and B-integral has been characterized for the 1ω beam [5], and it is of further interest to determine how this structure is transferred through the frequency converter. The distribution of energy in this regime defines the local irradiance in the near field that drives small-scale ripple growth in the final optics, and directly determines the irradiance distribution in the far field "seen" by the target. Measurements in the two regimes require different diagnostic techniques, and are described separately below.

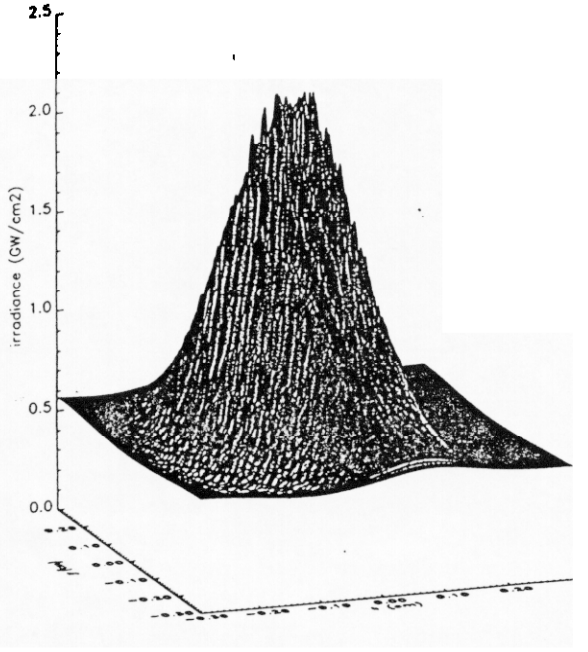

Figure 2. 3ω irradiance distribution in a small near-field patch showing ripple scale lengths of interest in the measurement of beam quality (simulation by W. Williams).

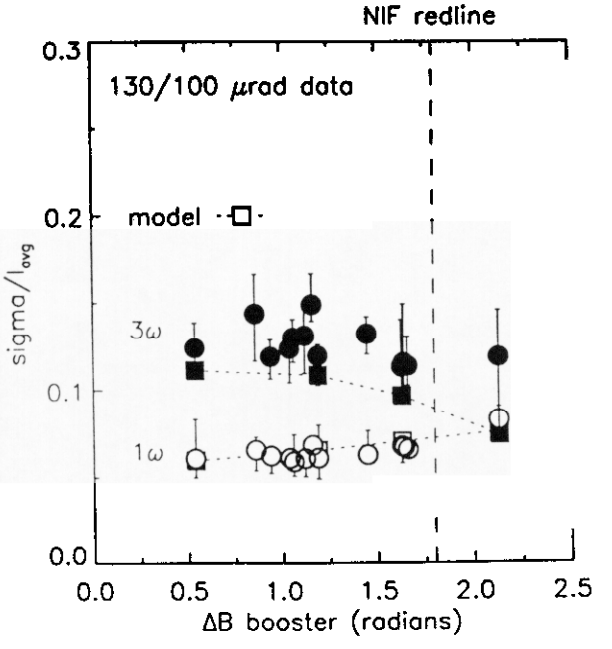

Figure 3. Plot of irradiance contrast versus B-integral accumulated in the booster amplifier stage. Open and filled circles denote measured values of 1ω and 3ω contrast respectively, for the case of ± 130 μrad filtering in the cavity and ±100 μrad filtering in the transport. Squares denote simulations.

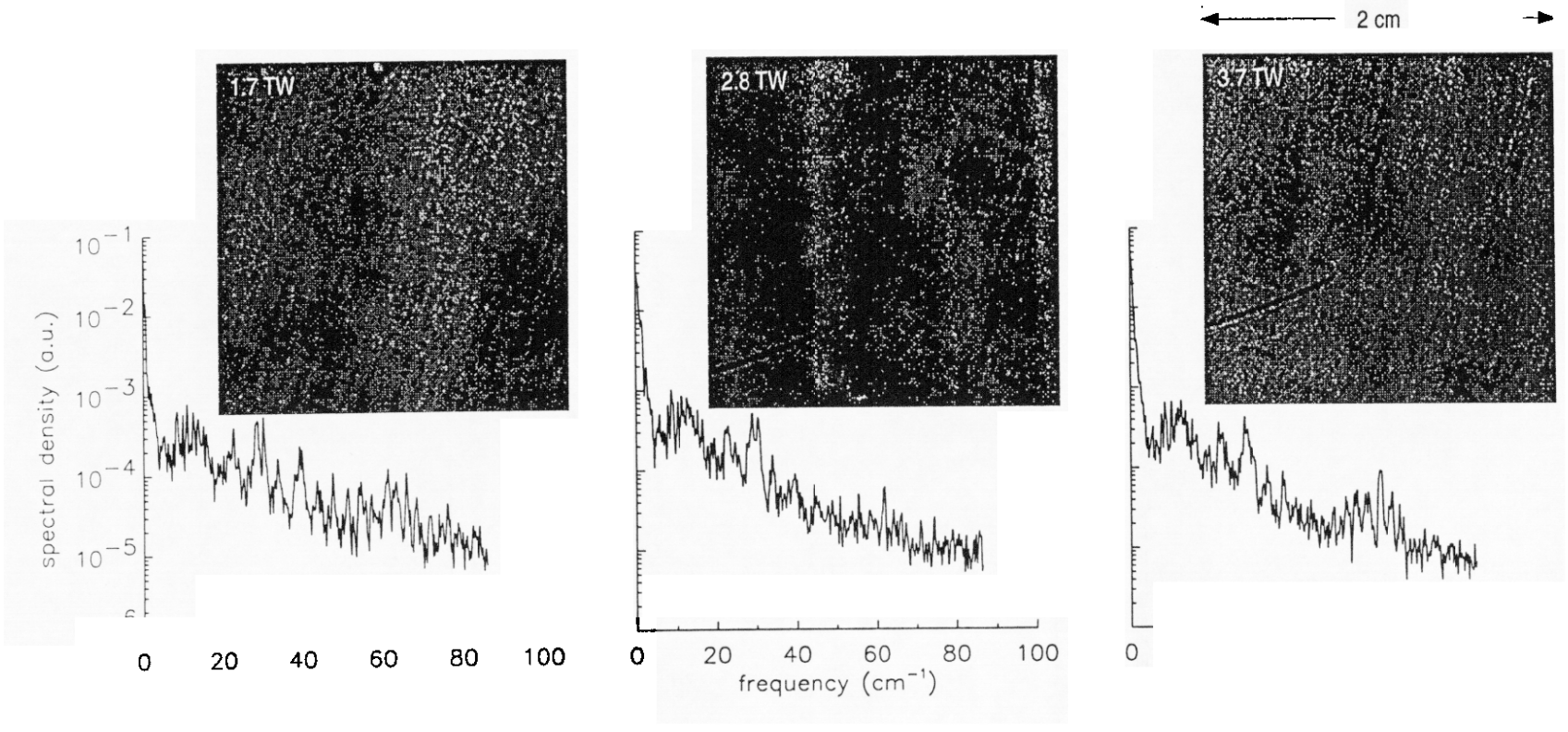

Figure 4. Spectral analysis of beam modulation associated with crystal surface finish, at different 3ω power levels (see text).

A parameter that has proven useful for describing near-field modulation at the longer ripple scale lengths is the irradiance contrast, defined to be the standard deviation of the irradiance distribution divided by the mean. To determine the 3ω irradiance contrast, the near-field irradiance (fluence divided by the effective pulse width) of the 34-cm beam was imaged at a plane near the final focus lens with ~ 2-mm spatial resolution using a scientific-grade CCD camera. The irradiance statistics were analyzed in 5-cm patches at several locations in the aperture that avoided the edges of the beam and the 'detuned' regions shown in Figure 1(a). The average contrast was determined from the patches and is plotted in Figure 2 versus ΔB, or the B-integral accumulated in the booster amplifier stage. The data was obtained using ±130 μrad and ±100 μrad acceptance-angle pinholes in the cavity and transport spatial filters, respectively. Error bars in the plot indicate the range of contrast values encountered in the analysis of the different patches. The data is plotted versus ΔB in the booster because calculations and experiments have shown this to be the critical parameter that determines power-dependent growth of the 1ω contrast [5]. The 1ω contrast obtained from patch analysis of the 1ω irradiance at the entrance to the crystals is also plotted for comparison.

The data indicates that the irradiance contrast approximately doubles on frequency tripling, with the contrast at the third harmonic actually being highest at low ΔB (low power). At low power, the conversion efficiency is a rapidly-increasing function of the 1ω drive irradiance, which causes fluctuations in the 1ω irradiance to become exaggerated at 3ω. At high power, the conversion efficiency tends to saturate at a near- constant percentage of the drive irradiance, resulting in the 1ω and 3ω contrast values being more similar. Modeling confirms this conclusion, as shown by the dashed curves in the plot connecting contrast values calculated from Beamlet simulations. The measured and modelled values for 3ω contrast agree to within ~20% up to the NIF red-line ΔB of 1.8 radians; at higher ΔB, the spatial non-uniformity of the frequency converter makes comparison difficult. At red line, the estimated peak-to-mean modulation based on contrast is 1.3 to 1.5:1. Clearly, improved crystal quality will be needed to ensure that equivalent modulation levels can be maintained across the entire aperture. Contrast at the third harmonic was also measured for ±200-μrad pinholes in both cavity and transport filters and found to be similar, within error bars.

To evaluate the threat of 3ω filamentation associated with near-field modulation at the smaller scale lengths we used a special film-format camera having a measured near-field resolution of <70 μm [10,16]. At a 3ω power level of 3.5 TW, assuming 1.5:1 modulation and a nonlinear coefficient for silica of 3.5×10^{-7} cm^2/GW [11], the optimum scale lengths for nonlinear ripple growth in the final lens range from 45 to 70 cm^{-1}. The Fresnel length for this size structure is only a centimeter or so, therefore special care was taken with the setup of the camera to ensure that the exit surface of the lens was imaged to within ±1 mm so that any localized small-scale beam breakup occurring in the lens could be observed before it became significantly modified by diffraction. The wedged thickness of the lens provided the additional diagnostic advantage of an approximately-linear 4:1 variation in B-integral across the beam, with the peak value incurred in these tests estimated at ~1.5 radians. Full aperture images, de-magnified to ~14 cm square, were obtained on Kodak 4421 Aerographic film, from which representative 2-cm square patches (5 cm equivalent) were digitized with equivalent 50-μm resolution using a microdensitometer. Determination of the film's characteristic curve and the conversion of film density to laser exposure was accomplished using standard techniques. Examples of high-resolution near-field data obtained from a single patch located on the thick side of the lens , but at successively higher power levels, are shown in Figure 3. The cross-hatching visible in the images corresponds to intensity modulation caused by the four diamond-turned crystal surfaces. A spectral analysis of the modulation in each patch was performed after first modifying the images for zero piston, unit normalization, and the application of a Hanning window. A portion of the resulting two-dimensional Fourier spectrum associated with one of the sets of diamond turning lines was extracted by means of line scans and is reproduced in the Figure. The results indicate that power-dependent growth of small-scale ripple is negligible, even at power levels exceeding SBSS levels (when scaled for the Beamlet aperture). The results are supported by apertured-calorimetry measurements which detected no discernible power-dependent increase in the fractional energy content outside of 200 μrad.

Although small-scale beam breakup associated with the crystal finish does not appear to be an issue, nonetheless a total of ten isolated filamentation tracks were observed in the lens following shots at power levels above 3.1 TW. In all cases, the tracks occurred on the thick side of the lens in locations exhibiting small (~150 μm diameter) pre-existing damage on the lens *exit* surface. The surface damage was incurred in earlier experiments conducted at lower power levels but higher fluence, suggesting the existence of localized hot spots in the 3ω beam, most likely caused by small defects on the exit surface of the tripler. This hypothesis has yet to be confirmed pending the development of a side-illuminated inspection system for the crystals similar to that currently in use on the lens.

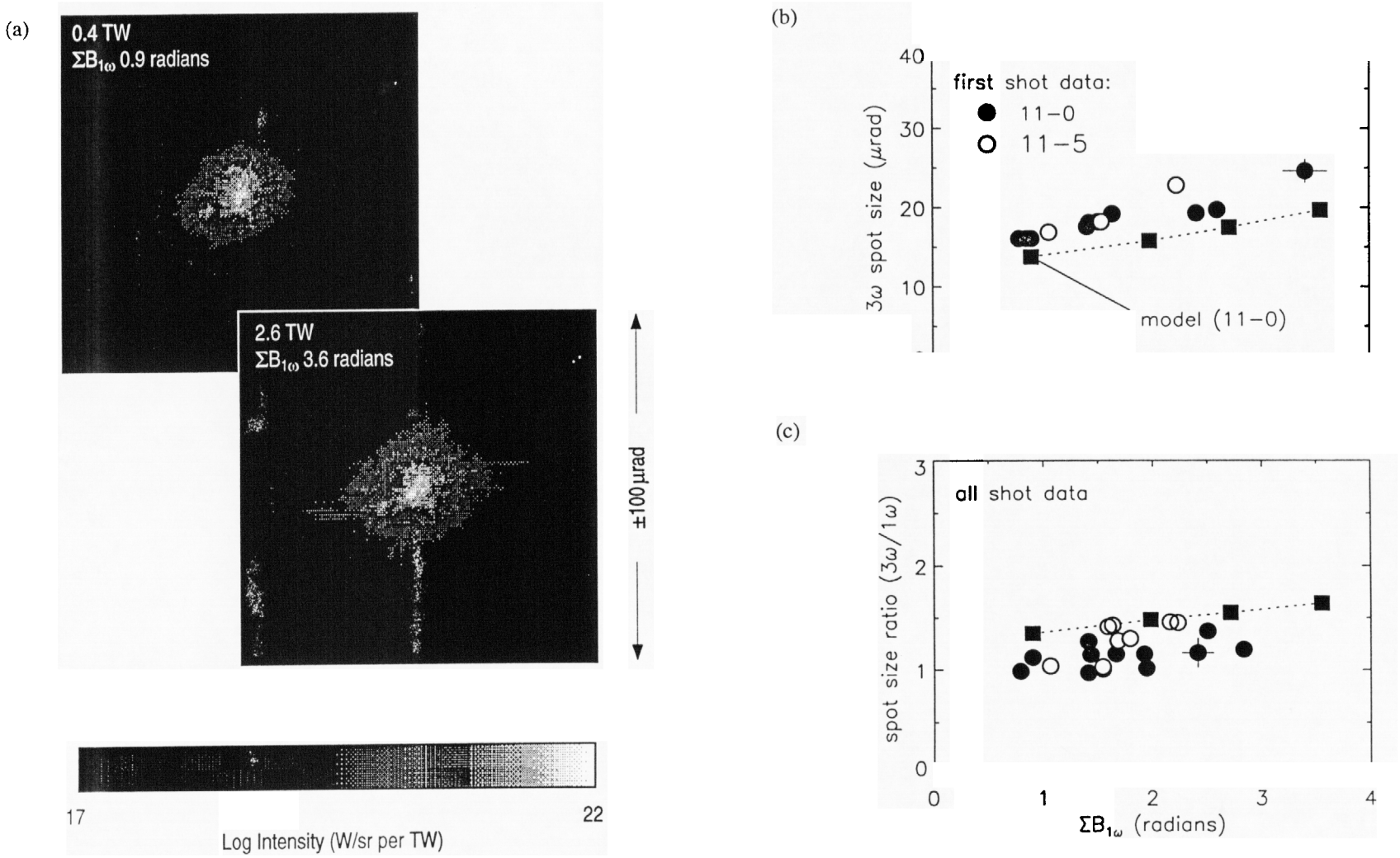

Figure 5(a). Measured angular distribution of 3ω power produced at different levels of system B-integral. Irradiance at the equivalent target plane is equal to the intensity divided by the square of the lens focal length (700 cm) and multiplied by the peak 3ω power indicated. (b) and (c) 3ω spot size (defined in text) and the ratio of 3ω spot size to 1ω spot size measured for different amplifier configurations, plotted versus total 1ω B-integral.

4. FAR FIELD BEAM QUALITY

Far-field beam quality was evaluated to ascertain compliance with NIF focal-spot specifications. The measurements were obtained with a 16-bit scientific-grade CCD camera that imaged the focused laser irradiance at the equivalent 3ω target plane with a resolution of ~1 μrad/pixel. A film-format camera of afocal design imaged multiple planes in the vicinity of the equivalent target plane to verify the acquisition of best focus. A second scientific-grade camera located in the Beamlet 1ω diagnostics package [17] measured the far-field irradiance distribution at the input to the frequency converter for comparison. Wavefront was controlled with the Beamlet adaptive optics system, which consists of a deformable mirror configured closed-loop to a wavefront sensor located in the output 1ω diagnostics package. The control loop remained closed until one second prior to shot time [18]. With the mirror prefigured to offset pump-induced distortions in the laser amplifier, the output wavefront as measured with a 247-element Hartman sensor ranged from 1 to 1.5 waves peak to valley, with an RMS error of ~.25 waves.

Figure 5(a) shows examples of 3ω far-field intensity distributions measured at both low and high power, demonstrating the characteristic 'flaring' of the focal spot that is observed at high B-integrals. With the exception of a few percent of the energy, the measured distributions are seen to fall well within the pass band of the 1ω spatial filters, therefore it is the total accumulated B in the laser system (ΣB as opposed to ΔB) that should be considered when discussing divergence. A useful quantifier of divergence is the half angle that encompasses 80% of the total power, referred to here as the spot size. For these measurements the fractional power was normalized to the total power contained inside the ±200 μrad field of view of the camera, with the acceptance angle of the camera designed to be the same as that of the target laser entrance hole. Figure 5(b) plots the measured 3ω spot size versus ΣB. The plot was compiled from data obtained on the first shot of each test day to avoid measuring divergence associated with thermal loading of the amplifier slabs [9,19]. The data shows that the spot size increases roughly as $B^{1/3}$ from a value of ~17 μrad at low power (ΣB of 0.8 radians) to a value of 25 μrad at a NIF red-line B of 3.6 radians. The size of the 1ω focal spot was found to be similar, with the spot size ratio (3ω/1ω) ranging from approximately 1 to 1.5 for all shots measured (see Figure 4(c)). The Beamlet simulations, which include diffraction in the frequency converter model, predict spot size values within ~20% of those observed.

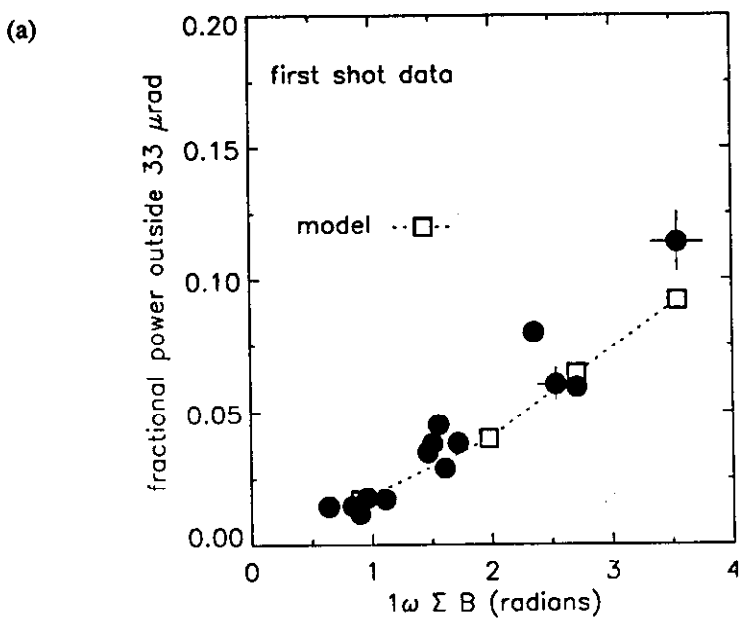

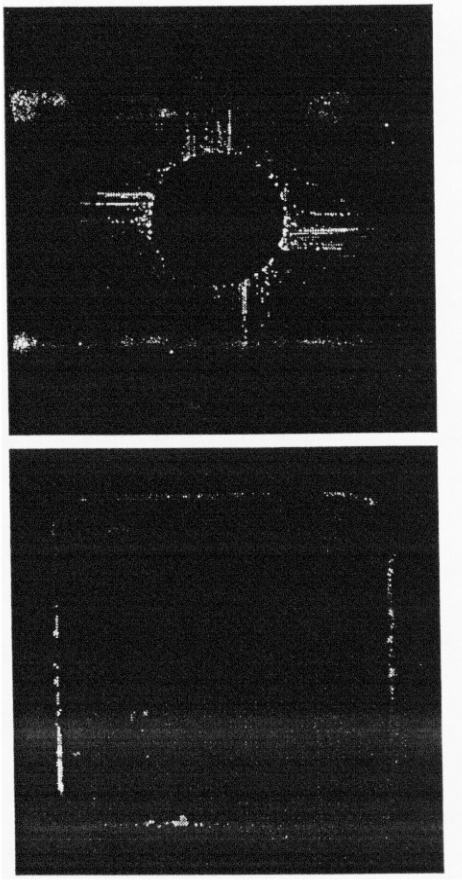

Figure 6(a). Plot of fractional 3ω power measured outside of 33 μrad versus the B-integral accumulated in the 1ω laser. (b) Photograph of a 2.6 TW 3ω beam at the plane of the ±33-μrad obscuration (ΣB = 3.6 radians). (c) Corresponding dark-field image showing regions of high divergence in the near field.

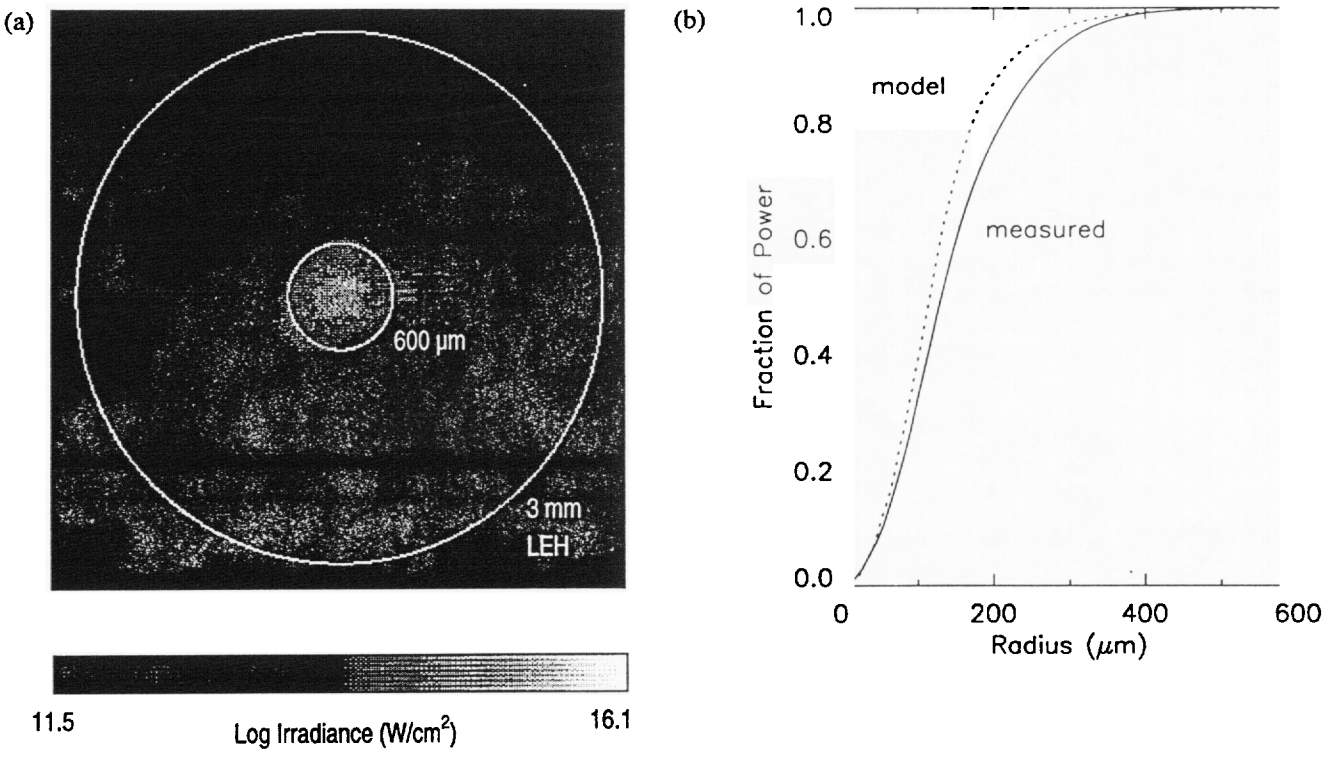

Figure 7(a). 2.1 TW 3ω focal spot produced by a 16-level kinoform phase plate. Size of the target laser entrance hole (LEH) is indicated for comparison. (b) Radial distribution of power inside the LEH.

Dark-field measurements suggest that the power-dependent increase in spot size depicted in Figure 5(b) is primarily a result of whole-beam self focusing. The measurements were performed by placing a ±33-μrad obscuration at a tertiary 3ω focus produced by the diagnostics. The fraction of 3ω energy passed around the obscuration was measured and is plotted as a function of ΣB in Figure 6(a). Again, only data from the first shot of a day is shown to avoid complications associated with amplifier thermal effects. At the highest ΣB tested (3.6 radians) the fraction approached 12%, with the majority of the energy contained in the flare-like structure of the focal spot mentioned above (see Figure 6(b)). Analysis of the near-field irradiance at a plane equivalent to the final focus lens (Figure 6(c)) reveals that 80% of the energy passed around the block originates at the edges of the beam. The B-dependence and the concentration of divergence at the edges of the beam are signatures of whole-beam self focusing. The dominant contribution comes from the 1ω laser, since each radian of phase retardation incurred at the edges of the 1ω beam is tripled to 3 radians upon frequency conversion, making the B added by passage through the 3ω optics small by comparison.

The quality of the focal spot generated with a kinoform phase plate (KPP) was tested to compare Beamlet performance with ICF specifications. As shown in Figure 7, the 3ω focal spot produced at a power level corresponding to the NIF red line (scaled for the Beamlet aperture) closely approaches the base-line ICF criteria for laser irradiance inside the target LEH. Specifically, 95% of the energy inside the LEH is within 600 μm, the 1/e radius of the spot is < 250 μm, and the irradiance at the edge of the LEH is below 10^{14} W/cm^2. The presence of high-angle structure associated with whole-beam self focusing, however, prevents the focal spot from meeting the super-Gaussian profile criteria specified for the NIF.

5. CONCLUSION

Third-harmonic performance of the Beamlet prototype laser has been tested up to and exceeding NIF red-line specifications for output irradiance and system B-integral. Measurements of converter efficiency obtained at 1ω drive irradiances up to 5.6 GW/cm^2 have provided valuable feedback for the NIF component development effort. Efficiencies of >80 % were verified over a significant portion of the 34-cm beam aperture, however the spatial uniformity of the crystal birefringence was revealed as an issue which must be addressed. The threshold for 3ω filamentation in the final optics was tested with a NIF specification crystal finish and found to be adequate for operation up to 3.5 GW/cm^2 (lower bound). The angular distribution of the 3ω beam was also measured and found to be in nominal agreement with ICF specifications, but ~ 50% larger than the divergence goal set for the NIF weapons physics mission. It is estimated that a 20% improvement in divergence at low power may be attainable through wavefront optimization of the 1ω beam. However, scattered energy fractions of ~10% outside of 33 μrad are expected to remain a lower limit at high power, unless a reduction in whole-beam self focussing can be achieved through improved edge apodization.

6. ACKNOWLEDGMENTS

We would like to acknowledge the Beamlet operations team for their crucial role in conducting these experiments. The B-integral calculations for Beamlet were performed by C. Clay Widmayer. The 16-level kinoform phase plate used in the tests was fabricated by Michael C. Rushford, Jerald A. Britten and Ian M. Thomas. We also wish to thank John T. Hunt of the NIF project for his helpful advice and guidance. This work was performed under the auspices of the U.S. Department of Energy by Lawrence Livermore National Laboratory under contract No. W-7405-ENG-48.

7. REFERENCES

1. *National Ignition Facility Conceptual Design Report, Volume 2: Design Basis and Requirements,* p. 3-41, UCRL-PROP-117093 Vol 2, Livermore, CA, (1994).

2. T. S. Perry, B. H. Wilde, "NIF system-design requirements for nuclear-weapons physics experiments", UCRL-ID-120738, Livermore, CA, (1995).

3. S.N. Dixit, M. C. Rushford, I. M. Thomas and M. D. Perry, "Continuous contour phase plates for tailoring the focal plane irradiance profile," *Proc. Soc. Photo-Opt. Instrum. Eng.*, **2633**, 141 (1995).

4. B. M. Van Wonterghem, J. R. Murray, J. H. Campbell, D. R. Speck, C. E. Barker, I. C. Smith, D. F. Browning and W. C. Behrendt, *ICF Quarterly Report*, Lawrence Livermore National Laboratory, Livermore, CA, UCRL-LR-105821-95-1, **5**, 1 (1994).

5. C.C. Widmayer, J.M. Auerbach, R.B. Ehrlich, M.A. Henesian, J.T. Hunt, J. K. Lawson, D. Milam, P. A. Renard, D. R. Speck, P. J. Wegner, T. L. Weiland, W. H. Williams, C. R. Wolfe and B. M. Van Wonterghem, "Producing National Ignition Facility (NIF) quality beams on the Nova and Beamlet lasers," 12th Topical Meeting on the Technology of Fusion Energy, Reno, Nevada, June 16-20, 1996. To be published.

6. B. M. Van Wonterghem, P. J. Wegner, J. K. Lawson, M. A. Henesian, J. M. Auerbach, C. E. Barker, D. R. Speck, C. E. Thompson and J. A. Caird,"Recent performance results from the National Ignition Facility Beamlet demonstration project," 12th Topical Meeting on the Technology of Fusion Energy, Reno, Nevada, June 16-20, 1996. To be published.

7. J. T. Salmon, E. S. Bliss, J. L. Byrd, M. Feldman, M. A. Kartz, J. S. Toeppen, B. Van Wonterghem and S. E. Winters, "An adaptive optics system for solid-state laser systems used in inertial confinement fusion," *Proc. Soc. Photo-Opt. Instrum. Eng.*, **2633**, 105 (1995). B. M. Van Wonterghem, J. T. Salmon and R. W. Wilcox, *ICF Quarterly Report*, Lawrence Livermore National Laboratory, Livermore, CA, UCRL-LR-105821-95-1, **5**, 42(1994).

8. A. C. Erlandson, M. D. Rotter, D. N. Frank and R. W. McCracken, *ICF Quarterly Report*, Lawrence Livermore National Laboratory, Livermore, CA, UCRL-LR-105821-95-1, **5**, 18 (1994).

9. J. M. Auerbach, D. Eimerl, D. Milam and P. W. Milonni,"A perturbation theory for electric field amplitude and phase ripple transfer in frequency doubling and tripling," UCRL-JC-124005, Livermore, CA, (1996). Submitted to Applied Optics.

10. P. J. Wegner, B. M. Van Wonterghem, S. N. Dixit, M. A. Henesian, C. E. Barker, C. E. Thompson, L. G. Seppala andJ. A. Caird,"Characterization of third-harmonic target plane irradiance on the National Ignition Facility Beamlet demonstration project," 12th Topical Meeting on the Technology of Fusion Energy, Reno, Nevada, June 16-20, 1996. To be published.

11. D. Milam, J. T. Hunt, K. R. Manes and W. H. Williams,"Modeling of filamentation damage induced in silica by 351-nm laser pulses," Annual Symposium on Optical Materials for High Power Lasers, Boulder, Col, Oct 7-9, 1996. To be published.

12. R. S. Craxton, "High efficiency frequency tripling schemes for high power Nd:glass lasers," *IEEE J. Quantum Electron.* **QE-17**, 1171 (1981).

13. P. J. Wegner, M. A. Henesian, D. R. Speck, C. Bibeau, R. B. Ehrlich, C. W. Laumann, J. K. Lawson and T. L. Weiland, "Harmonic conversion of large-aperture 1.05-μm laser beams for inertial-confinement fusion research," *Appl. Opt.* **31**, 6414 (1992).

14. C. E. Barker, J. M. Auerbach, C. H. Adams, S. E. Bumpas, R. L. Hibbard, C. L. Lee, D. H. Roberts, J. H. Campbell, P. J. Wegner, B. M. Van Wonterghem and J. A. Caird, "National Ignition Facility frequency converter development," Paper 5-3 this proceedings.

15. M.S. Webb, D. Eimerl and S. P. Velsko,"Wavelength insensitive phase-matched second-harmonic generation in partially deuterated KDP," *J. Opt. Soc. Am.* **9**, 1118 (1992). D. Eimerl,"Electro-optic, linear and nonlinear optical properties for KDP and its isomorphs," *Ferroelectrics* **72**, 95 (1987).

16. J. A. Caird, H. G. Patton, L. G. Seppala, C. E. Thompson and P. J. Wegner,"Beamlet focal plane diagnostic," Paper 6-4 this proceedings.

17. S. C. Burkhart, W. C. Behrendt and I. Smith, *ICF Quarterly Report*, Lawrence Livermore National Laboratory, Livermore, CA, UCRL-LR-105821-95-1, **5**, 68 (1994).

18. M. W. Kartz, W. C. Behrendt, R. G. Hartley, A. F. Hinz, G. G. Pollock, E. S. Bliss, J. T. Salmon and S. E. Winters,"Wavefront correction for static and dynamic aberrations to within 1 second of the system shot in the NIF beamlet demonstration facility," Paper 8-1 this proceedings.

19. M. D. Rotter, R. W. McCracken, A. C. Erlandson and D. Brown, "Thermal recovery measurements on multi-segment amplifiers," *Proc. Soc. Photo-Opt. Instrum. Eng.*, **2633**, 70 (1995).